Volume 17, Number 2, 2024. pp. 135-145

Jordan Journal of Physics

ARTICLE

Silver Prism Interface Surface Plasmon Resonance (SPR) for Biosensor in UV-Visible Spectrum Region

Farah J. Kadhum[a], **Sahar A. Mohammed**[a], **Shaymaa H. Kafi**[a], **Ali A. Al-Zuky**[a], **Mahasin F.Hadi Al-Kadhemy**[a] and **Anwar H. Al- Saleh**[b]

[a] *Physics Department,College of Science,Mustansiriyah University, Baghdad, Iraq.*

[b] *Department of Computer Science, College of Science, Mustansiriyah University, Baghdad, Iraq.*

Doi: **https://doi.org/10.47011/17.2.1**

Received on: 01/08/2022; *Accepted on: 04/10/2022*

Abstract: Surface plasmon resonance (SPR) sensors have been extensively employed in biological and chemical detection because they can carry out simple, direct, extremely sensitive, and in-the-moment detection. They can be used to create a simulation model for different silver (Ag) layer thicknesses (d_{Ag}) deposited on a semicircular glass prism. The D-ZLAF50 uses water as the sensing medium and can be turned on by an evanescent generated by total internal reflection on the sensor surface in the Kretschmann setup. The SPR phenomenon cannot be noticed in the ultraviolet area using the simulation technique for the suggested sensor. However, it can be seen faintly in the visible region, starting at wavelengths of 600 and 700 nm. Also, the simulation results show that this sensor, demonstrating operational stability, can be used in the visible region of the spectrum at a wavelength of 600 nm. When an aqueous sensor is used to detect any changes in the refractive index by an amount $\Delta n \geq 0.02$, the sensitivity values fall in the range of $S = 134 - 140$. The length of the SPR dip is close to L_d = 0.9, and FWHM values range between 6.6° and 6.8^o when the thickness d_{Ag} varies from 10 to 80 nm.

Keywords: SPR, Surface plasmon resonance, Optical biosensor, Biosensors, Sensing applications

Introduction

Over the past two decades, surface plasmon resonance (SPR) has evolved from a somewhat obscure physical phenomenon to a commonly utilized optical tool in physical, chemical, and biological research that requires interface characterization [1]. Surface plasmons (SPs) need the presence of free electrons at the interface of two materials, and in practice, one of these materials is nearly invariably a metal with a high concentration of free conduction electrons. This is a natural result of applying Maxwell's equations to analyze a metal-dielectric interaction. SPs may be thought of as propagating electron density waves at the metal-dielectric interface or as electromagnetic (EM) waves closely associated with this interaction [2]. SP experiments with electron beam excitation began in 1968. The optical excitation was shown by Otto, Kretschmann, and Rather. Affinity biosensors based on SPR were the first sensing instruments and systems to be commercialized because of the adaptability of this method. However, affinity biosensors have several drawbacks, not the least of which is the high cost of the instruments and sensor chips [3]. Some light is reflected off the contact when a light beam goes from a material with a high refractive index (RI), such as glass, to a material with a low RI, such as water. The light is fully reflected (total internal reflection) when the angle at which the light reaches the contact (the angle of incidence) is greater than the critical

Corresponding Author: Ali A. Al-Zuky **Email**: Prof.alialzuky@uomustansiriyah.edu.iq

angle. The intensity of reflected light becomes a minimum (or zero) at a second angle greater than the critical angle, where the loss is greatest. The reflection is not perfect when a tiny coating of metal (such as silver Ag) is added to the glass; some light is absorbed by the metallic film [4].

Several researchers have developed SPR sensor devices that can detect changes in the material's optical characteristics under investigation. Some of the most significant of these investigations are as follows.

In 2014, Al-Qazwini *et al.* based on Ag and a titanium dioxide (TiO_2) overlayer, created a unique bilayer SPR-based fiber-optic RI sensor [5]. Using a finite-difference time-domain technique, they quantitatively assessed the optimum thickness of the TiO_2 overlayer in the suggested sensor and compared its performance with those based on typical bimetallic layers of Ag and gold (Au) in aquatic conditions. They showed that using a TiO_2 overlayer significantly increased sensor performance. The TiO_2 overlayer provided a more cost-effective oxidation solution than Au and allowed for resonance frequency tweaking.

In 2016, Lin and Chena evaluated the ideal Ag and Au layer thicknesses (d_{Ag}) for creating low reflectance of the bimetallic film sensor with air and water analytes [6]. Their results showed that attaining the highest sensitivity and the shortest full width at half maximum (FWHM) for a bimetallic SPR sensor simultaneously was challenging because the highest sensitivity was found in the SPR with a single Au layer, while the shortest FWHM was found in the SPR with a single Ag layer.

Lin *et al.* presented a genetic algorithm-based design technique for a high-performance SPR biosensor [7]. They created an Au-Ag-TiO_2-graphene-based SPR biosensor and compared it to a standard Au-graphene-based SPR biosensor. The created biosensor had roughly three times the resolution of the typical one based on the same sensitivity.

In 2021, Kadhum *et al.* produced a water-sensing medium by layering Ag and titanium oxide on the semicircular glass prism D-ZLAF50 [8]. Their work offered a simulation analysis for the SPR sensor utilizing an Ag layer with a thickness of $10-80$ nm coated on half semicircular glass prism D-ZLAF50. They determined the best conditions for obtaining a good SPR for this system by analyzing reflectivity and incidence angle curves and determining the SPR properties (FWHM and height dip L_d) in the $100-700$ nm spectrum of EM waves using water as the outer sensing medium with changing RI (Δn=0, 0.02, 0.05, and 0.1).

Surface plasmon resonance is one of the spectacular visual phenomena caused by EM light waves that can be seen all over SPRs. The SPR is caused by the interaction of the incident p-polarized light wave with the free electrons on the metal-dielectric surface, resulting in oscillating SP waves (SPW). Using noble metals such as Ag, Au, and Cu stimulates the sensor response, as these metal elements provide more sensitivity in the material [9].

Biomolecules cause a change in the analyte's RI, which is reflected in the SPR output (optical) signal. As a result, SPR-based biological sensing is a complex technology that necessitates a multidisciplinary approach encompassing manufacturing, optical engineering, and even medical sciences. Surface plasmon resonance sensing technology is used in a variety of sectors, including pathology, food safety, and environmental monitoring [10]. Surface plasmon resonance has been considered a vital technology for a wide range of sensing applications over the last three decades. Biosensors frequently utilize SPR sensors [11]. Applications of SPR technology include bioimaging, chemical detection, water testing, aqueous sample detection, food safety, environmental monitoring, biological analyte detection, and gas detection. Moreover, SPR technology is also used in optoelectronic devices, such as optical tunable filters, optical modulators, film thickness monitoring, and SPR imaging, due to continuous advancements in the field [12].

There are two traditional types of prism-coupling-based SPR sensors: Kretschmann and Otto setups. Both operate on the principle of attenuated total reflection. Despite their widespread use due to their strong sensing capabilities, Kretschmann-based configuration SPR sensors have several drawbacks. These sensors are large and typically feature moving optical and mechanical components. As a result, they are stuck in place and useless for distant sensing [13]. Moreover, spectral-based measurement is costly to execute in practice, and the ability to reduce sensor size is restricted.

To overcome such possible difficulties, optical fiber-based SPRs have been created. Optical fibers are lightweight and easy to deal with. Furthermore, the optical fiber's flexible structure allows for significant sensor size reduction, which is advantageous for remote sensing applications. Surface plasmon resonance sensors based on optical fibers provide a higher dynamic range and resolution for detection, although they are constrained by limited acceptance angles. Various optical fiber SPR sensors have been detailed in both theoretical and practical works [14]. There are several techniques for calculating an SP's dispersion relation, which is a connection between the angular frequency and the wave vector k. In his seminal work on SPs, Raether derived the SP dispersion relation from fundamental principles using Maxwell's equations [15]. The complex reflection coefficient r_p for p-polarized light at any contact between two media can be described using Fresnel's equations. Consequently, the complex reflection coefficient may be collected [16].

$$\boldsymbol{r_p = \frac{E_i}{E_r} = |r_p| e^{i\varphi} = \left|\frac{\tan(\alpha-\beta)}{\tan(\alpha+\beta)}\right| e^{i\varphi}} \quad (1)$$

Here, E_i and E_r denote the incident and reflected electric fields, $\alpha, and\ \beta$ representing the incident and refracted angles of EMW, respectively, and $\boldsymbol{\varphi}$ is the phase difference between incident and refracted light rays. Furthermore, depending on the refractive indices of the materials involved, the reflected field undergoes a phase change relative to the incident field. Reflectance, defined as the ratio of reflected intensities [15], has the following relationship:

$$\boldsymbol{R_p = |r_p|^2} \quad (2)$$

Two special cases are given by Cardona [17]:

- When $\alpha + \beta = \pi/2$, the denominator of Eq. (1) grows very high and R_p becomes zero. The Brewster angle is defined as the point at which p-polarized light does not reflect.
- The other particular situation arises when $\alpha - \beta = \pi/2$: as a result of Eqs. (1) and (2).

R_p becomes infinite. For a very small E_i, there exists a finite E_r. This situation is similar to resonance. The dispersion connection may be deduced from this relationship between α and β if $\alpha - \beta = \pi/2$, then $cos\,\alpha = -sin\,\beta$ and $tan\alpha = k_{1x}/k_{1y} = n2/n1$. The wave vector components $k = (k_x, k_y)$ can be expressed as follows [18]:

$$\boldsymbol{k_x^2 = k_1^2 - k_{y1}^2 = k_1^2 - k_x^2 \frac{\varepsilon_1}{\varepsilon_2}} \quad (3)$$

$$\boldsymbol{K_x = \frac{\omega}{c}\sqrt{\frac{\varepsilon_1\varepsilon_2}{\varepsilon_{1+}\varepsilon_2}}\ \ and\ K_{yi} = \frac{\omega}{c}\sqrt{\frac{\varepsilon_i^2}{\varepsilon_{1+}\varepsilon_2}}} \quad (4)$$

where ε_1 and ε_2 are the dielectric constants of materials 1 and 2, respectively, and i =1 or 2.

The SPR dispersion equation for an interface between two half-infinite media is given by Eq. (4). Subsequently, the case where medium 2 is a metal can be investigated. As a result of the enormous number of free electrons in this medium, its dielectric constant 2 becomes negative at an angular frequency $\omega < \omega_p$ of p [16]:

$$\boldsymbol{\varepsilon_2(\omega) = 1 - \frac{\omega_p^2}{\omega^2}} \quad (5)$$

$$\boldsymbol{\omega_p = \sqrt{4\pi n_e e^2/m_e}} \quad (6)$$

where ω_p is the plasma frequency, n_e is the free electron density, and e and m_e are the charge and mass electrons, respectively.

Materials

The SPR sensor system was designed in this simulation study, as shown in Fig 1. Masahiro Yamamoto's SPR algorithm [19] was modified by using a wide range of EM wavelengths (100 to 700 nm) instead of a single wavelength. Changing the wavelength leads to a change in the refractive indices (RIs) of all materials used in this system. The system presented in this simulation study consists of the following components:

- **Prism:** a semi-circular glass prism made of D-ZLAF50 dense lanthanum flint glass.
- **Silver layer**: a silver film with a thickness of $10 - 80$ nm.
- **Sensing media**: water.

The refractive indices of three materials (Ag, water, and glass) as a function of wavelength ($100 - 700$ nm) were obtained from the website (https://refractiveindex.info). A hypothetical change in water's RI (Δn = 0, 0.02, 0.05, and 0.1) was also used, as this change in RI can reflect the effect of pollution in water.

This system has been adopted, and the SPR algorithm of Masahiro Yamamoto, modified in this study, has been applied. The algorithm mainly depends on Fresnel equations to calculate the reflectivity and transmittance coefficients between any two media. It was then generalized to calculate the total reflectivity of the proposed system. The equations for the reflectivity coefficient, r_p, and transmittance coefficient, t_p, are as follows [20]:

$$r_p = \frac{n_2 \cos\theta_i - n_1 \cos\theta_t}{n_2 \cos\theta_i + n_1 \cos\theta_t}, \quad t_p = \frac{2n_1 cos\theta_i}{n_2 cos\theta_i + n_1 cos\theta_t} \qquad (7)$$

where r_p and t_p are reflection and transmission coefficients, respectively, for p-wave polarization. n_1 and n_2 are the RIs for the incident wave media (1) and media (2), respectively. Finally, θ_i and θ_t are the incident and the refractive angles, respectively.

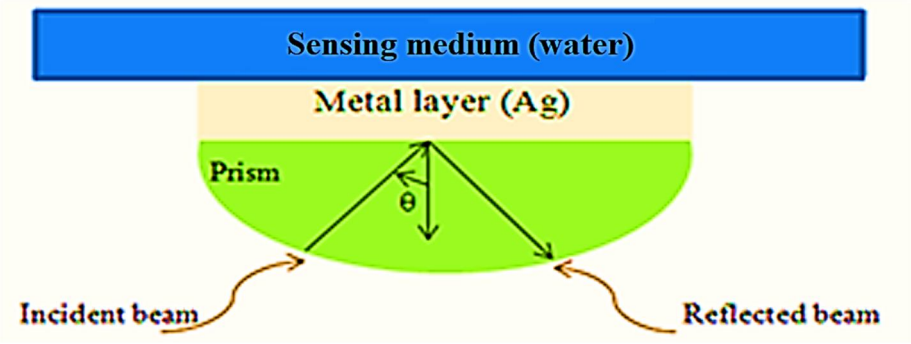

FIG. 1. The schematic diagram of surface Plasmon resonance sensors.

Figure 1 shows two interfaces: one between the prism and the Ag layer and the other between the Ag layer and the water. As a result, Fresnel equations must be applied twice. The developed SPR algorithm was designed using the MATLAB program.

Results and Discussion

The procedure for assessing reflectivity curve results in SPR techniques relies on two modes: angular interrogation mode SPR and spectral interrogation mode SPR [21]. This study concentrates on the first type of analysis using the simulation SPR MATLAB algorithm for λ=100 to 700 nm with a step change of 100 nm, changing in RI by Δn, and using an incident angle in the range of 0°–90° with a step change of 1°. The reflectivity curves obtained from this process are shown in Fig. 2. The metal's strong absorption, which rose dramatically for longer wavelengths, caused the SPR dip to spread as the resonance wavelength advanced. Angular measurements were also obtained to estimate the layers' true thicknesses and to construct the incidence angle for spectral measurements [22].

This study solely discusses the angular interrogation mode SPR. Figure 2 displays the reflectivity curves for Ag layer thickness changing from 10 to 80 nm in 10 nm increments. It can be recognized by the angle of the SPR. Surface plasmon excitation causes the most energy loss at the angle of incidence where the least reflection occurs. The following is a summary of the reflectivity curve's properties and the occurrence of SPRs:

- No angular interrogation mode θ_{SPR} appeared at d_{Ag} = 10 and 20 nm.
- Weak appearance of θ_{SPR} at λ= 600 and 700 nm for d_{Ag} = 30, 70, and 80 nm.
- Strong appearance of θ_{SPR} at 600 and 700 nm at d_{Ag} = 40 – 60 nm.

With a rise in the detection of changes in the medium's RI, the SPR angle changed somewhat towards higher values, which corresponds with previous findings [21]. The ideal film thickness of the metal-based SPR sensor produced an SPR reflectivity curve with a sensor structure that exhibited the greatest possible loss in reflectivity and the narrowest possible FWHM of the SPR dip. The length of the SPR dip was also substantial, and its value was close to one.

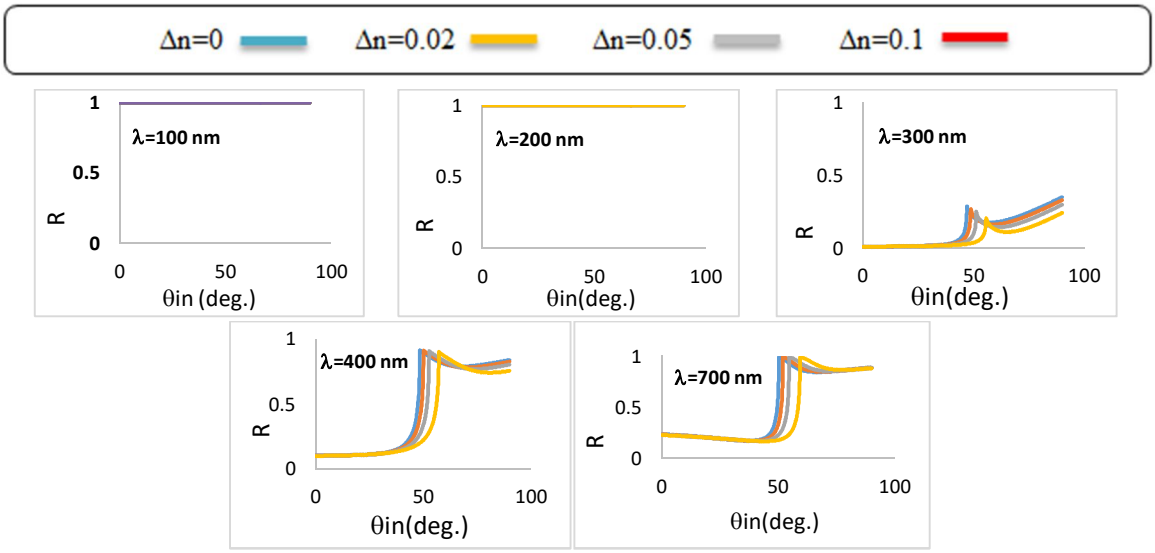

(a) d_{Ag}=10 nm

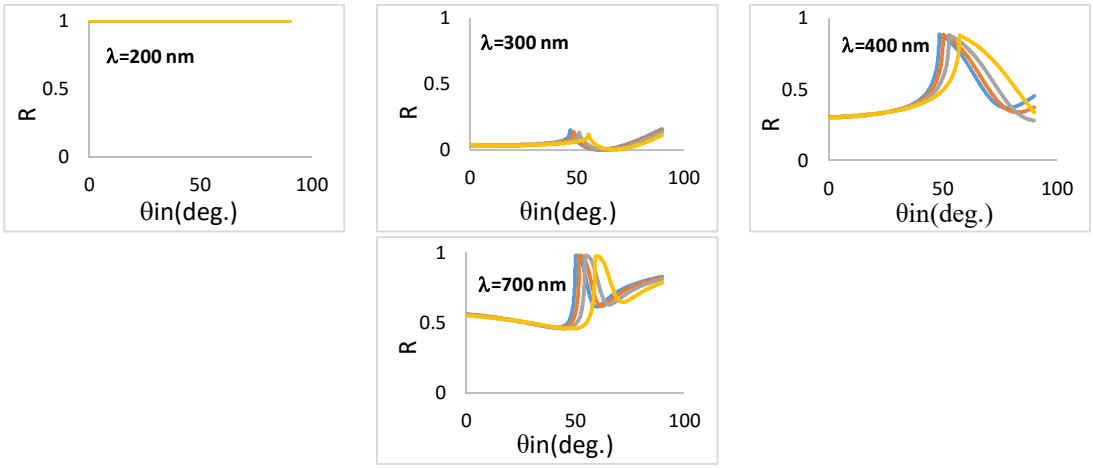

(b) d_{Ag}=20 nm

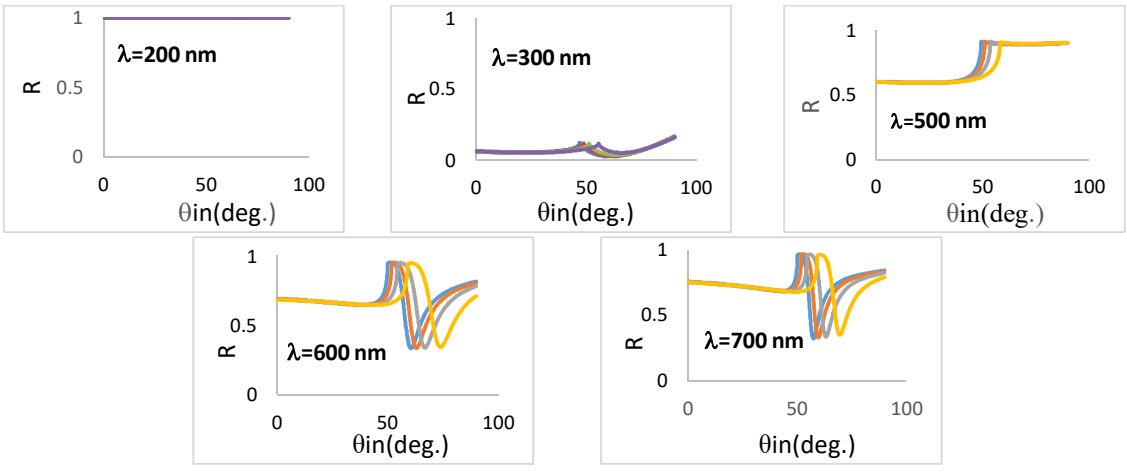

(c) d_{Ag}=30 nm

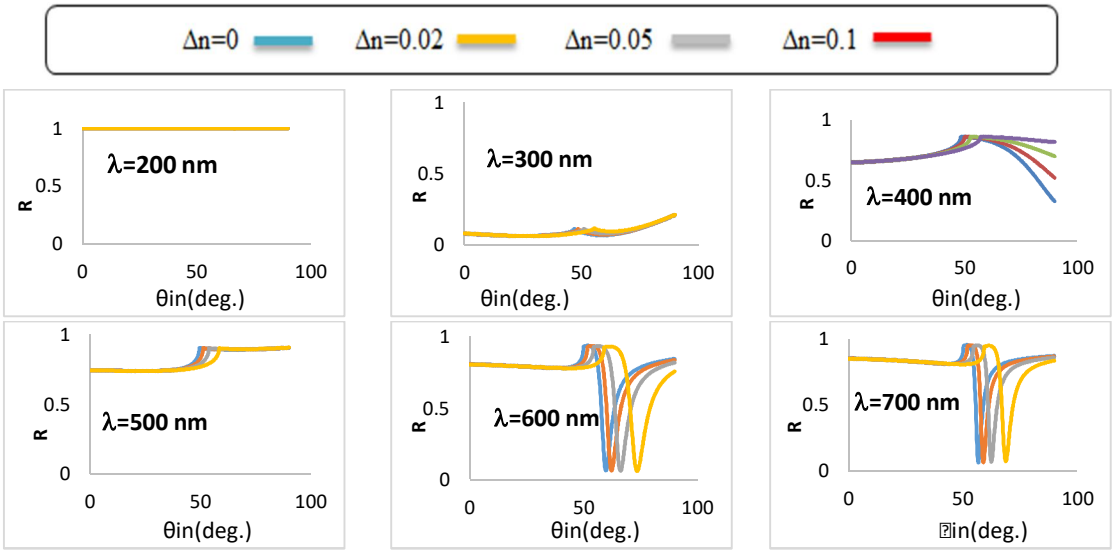

(d) d_{Ag}=40 nm

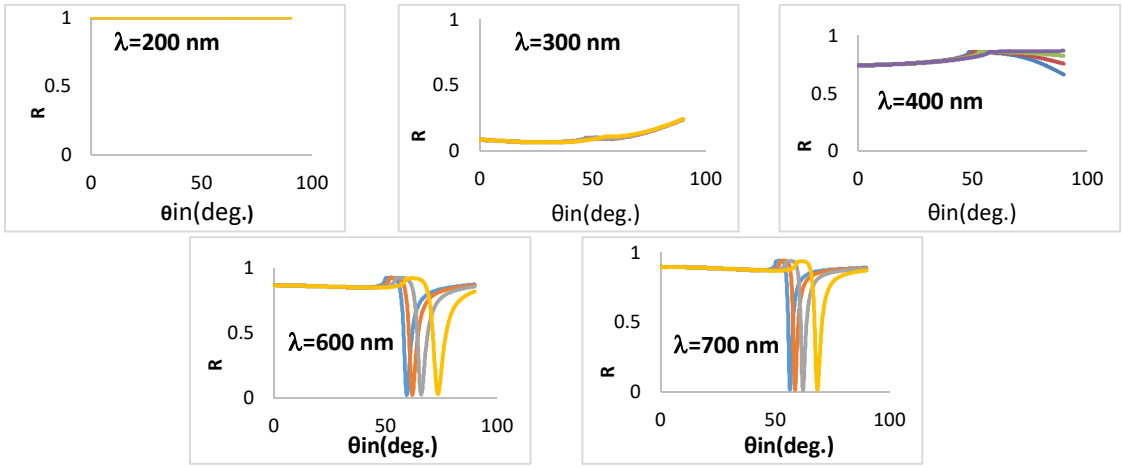

(e) d_{Ag}=50 nm

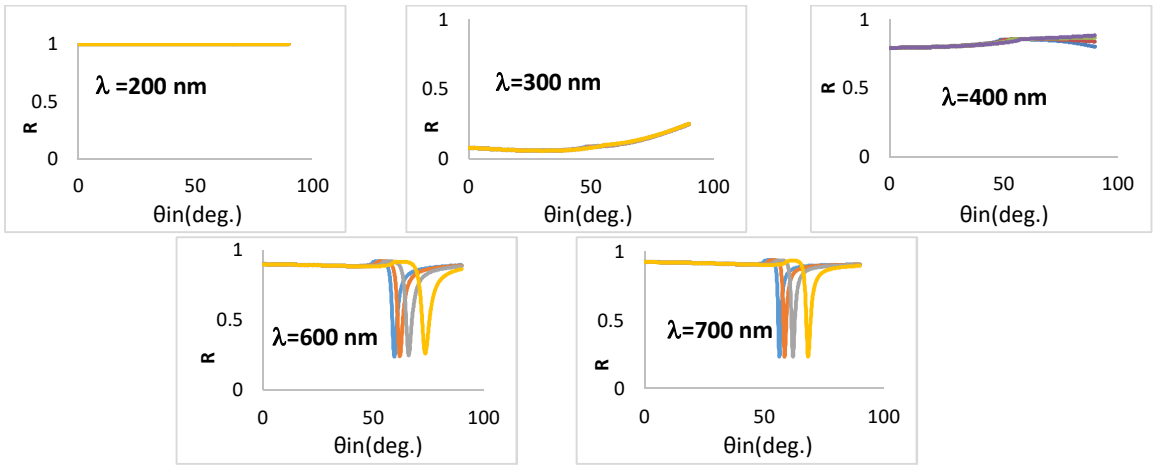

(f) d_{Ag}=60 nm

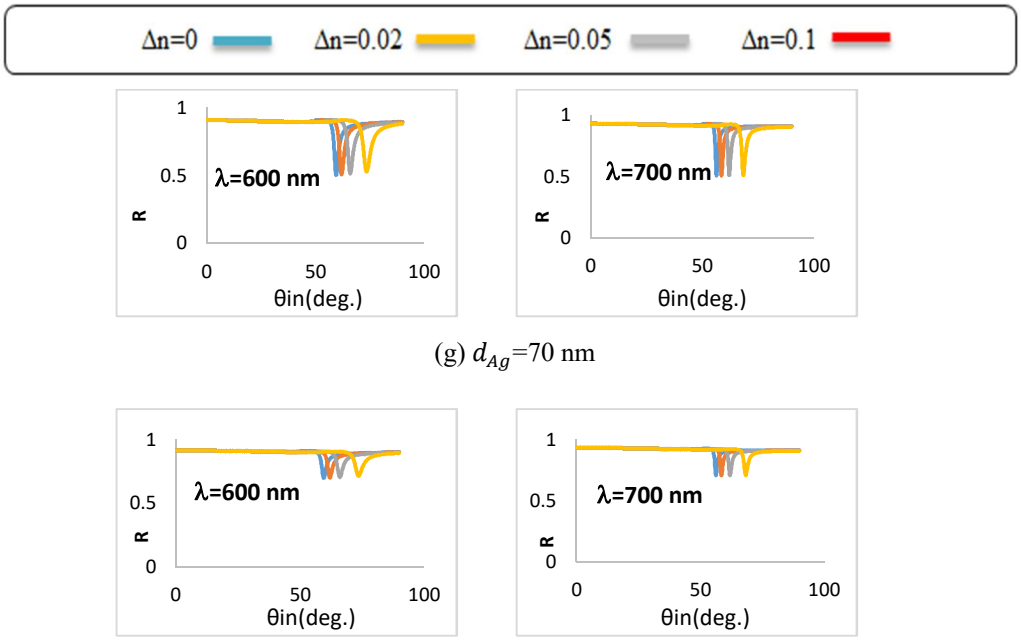

(g) d_{Ag}=70 nm

(h) d_{Ag}= 80 nm

FIG. 2. The relationship between the incidence angle and the reflectance at different wavelengths (200-700 nm) is illustrated for Ag layer thicknesses of (a) d_{Ag}= 10 nm, (b) d_{Ag} = 20 nm, (c) d_{Ag} = 30 nm, (d) d_{Ag} = 40 nm, (e) d_{Ag} = 50 nm, (f) d_{Ag} = 60 nm, (g) d_{Ag} = 70 nm, and (h) d_{Ag} = 80 nm.

The best SPR sensor computed sensitivity utilizing the estimated SPR dip attributes (FWHM and L_d), which provided a sharper FWHM and longer L_d. There is also another important parameter for calculating the quality of the sensor's work, which is the sensitivity parameter S, given by the following equation [23]:

$$\boldsymbol{S = \frac{\Delta\theta_{SPR}}{\Delta n}} \quad (8)$$

where $\Delta\theta_{SPR}$ represents the magnitude of the displacement in the surface plasmon resonance angle with a change in the refractive index by Δn.

The estimated FWHM and L_d of the SPR dip as a function of the outer change in medium RI (Δn) and wavelengths are shown in Fig. 3. At λ = 600 and 700 nm, the best results were as follows:

- The FWHM for the SPR dip is in the range of $5.7-8.5^o$ at d_{Ag} = 40 nm and λ = 600 nm, but at λ = 700 nm is reduced to $3.4-5.1^o$.
- Also, the FWHM decreased when the SPR dip rose with an increasing Δn at d_{Ag} = 50nm and λ = 600 nm to 1.9^o and fell to 3.1^o at λ = 700 nm.
- The FWHM decreased as the SPR dip rose with an increasing Δn at d_{Ag} = 60 nm and λ=600 nm to 1.4^o, while reduced to 2.3^o at λ = 700 nm.

In addition, the discovered L_d was semi-stable at all Δn values, with the best L_d being ≅ 0.9 for d_{Ag} = 40, 50, and 60 nm at λ (600, and 700 nm).

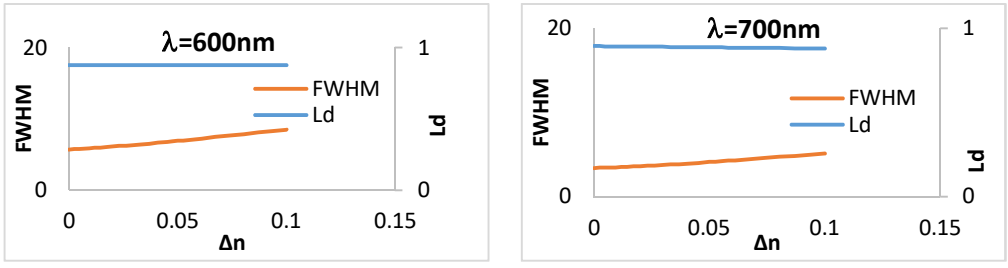

(i) d_{Ag} = 40 nm

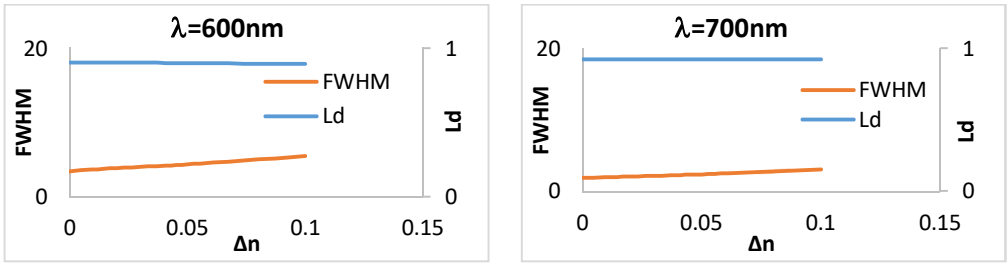

(ii) d_{Ag}= 50 nm

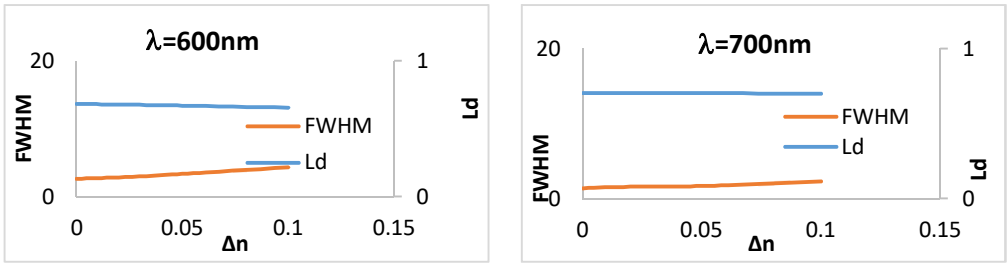

(iii) d_{Ag}= 60 nm

FIG. 3. The FWHM and L_d of thin film layers with changing refractive index for various wavelengths and thicknesses of Ag: (i) d_{Ag}= 40 nm, (ii) d_{Ag}= 50 nm, and (iii) d_{Ag}= 60 nm.

Figure 4 depicts the FWHM and L_d with altering Ag layer thicknesses for varied RI of thin film layers and wavelengths. The best FWHM values were found for the SPR dip length at 600 nm and Δn = 0.1, with an L_d of 0.9 recorded at both wavelengths (600 and 700 nm) [24].

In terms of the FHWM values, at Δn = 0.1 with the 600 nm wavelength within the range of $6.6–6.8^o$ in a change of $d_{Ag} = 40 – 60$ nm, the SPR dip became narrower by employing the 600 nm wavelength, where its value ranged between 6.8° and 1.8^o. The FWHM started to decline further, indicating that the SPR dip got narrower while utilizing the wavelength of 700 nm, and its FWHM value became steady with various d_{Ag} values.

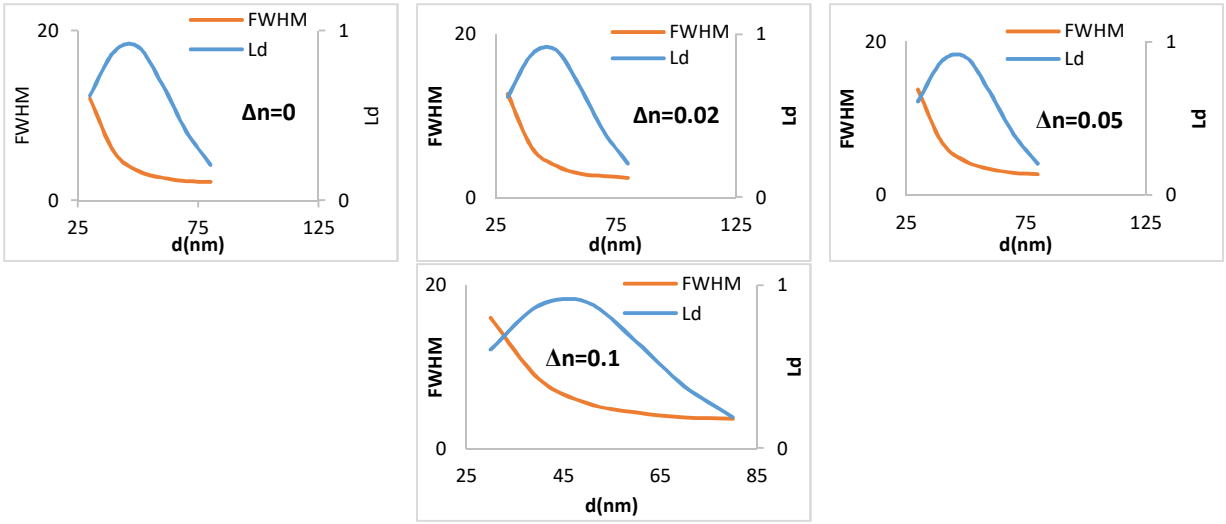

(a) λ= 600 nm

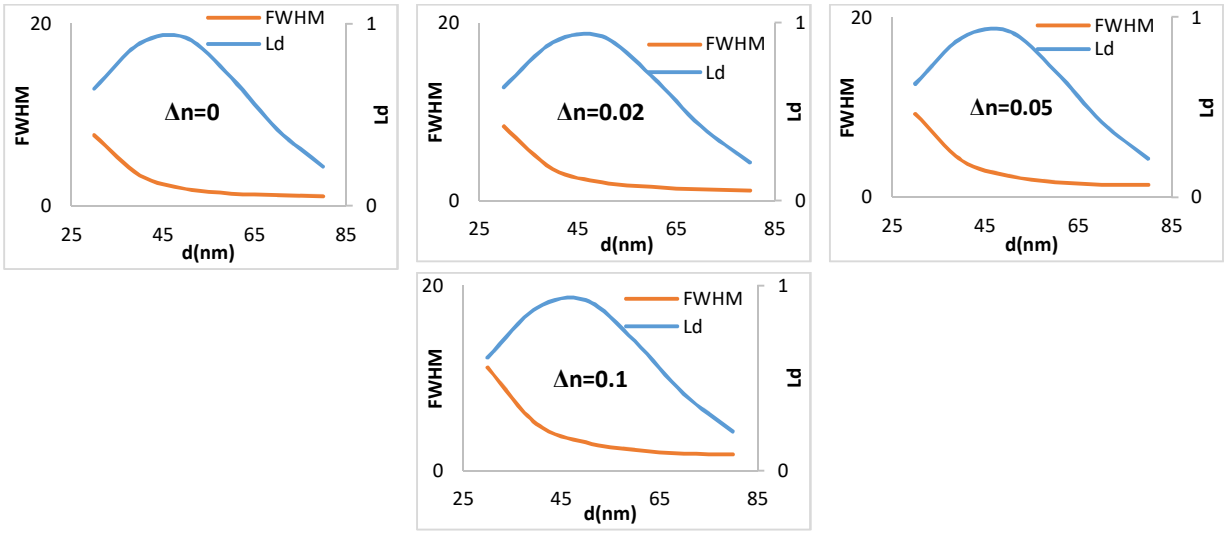

(b) λ = 700 nm

FIG. 4. The graph shows the FWHM and length dip L_d for different refractive indices of thin film layers and wavelengths when the thickness of the Ag layer is changed.

Figure 5 depicts the link between sensitivity related to changes in the Ag layer's thickness and the changes in refractive indices of the sensing medium (Δn). Sensitivity showed a semi-stable trend across all thickness ranges of the Ag layer, with peaks observed at 600 and 700 nm. Additionally, it should be noted that the sensitivity rose as the RI of the sensing medium Δn increased.

At Δn = 0.02, sensitivity values (S) were $S = 120 - 125$ and $S = 110 - 115$, at wavelengths of 600 and 700 nm, respectively, for thicknesses d_{Ag} between 10 and 80 nm. Also, at Δn = 0.05 and 0.1 at $\lambda = 600 - 700$ nm, the sensitivity (S) ranged from 115 to 140, which is consistent with [25]. This stability in sensitivity values as a function of silver thicknesses from 30 to 80 nm means that this sensor can operate efficiently within the silver layer thickness range.

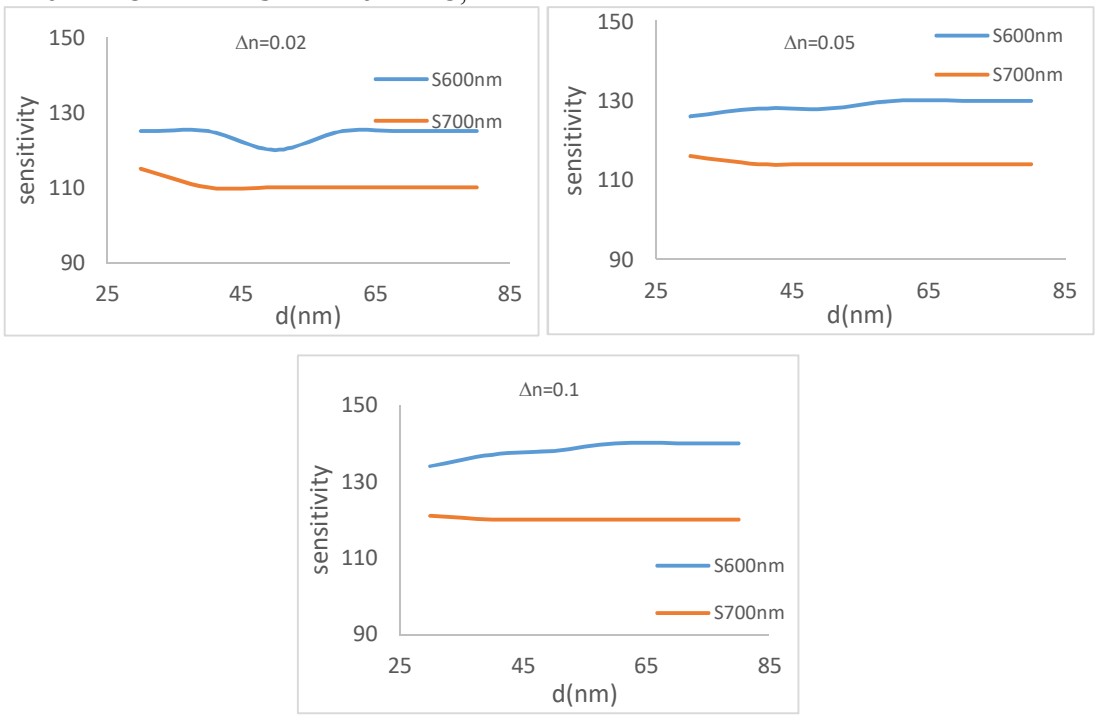

FIG. 5. The effect of the refractive index Δn on the sensitivity of the Ag layer thickness at different wavelengths.

Conclusion

From the simulation results of the proposed sensor, it is evident that the sensor obtained high sensitivity values, narrow FWHM, and L_d values close to one for dipping SPR, indicating the efficiency of the proposed system. So from the simulation results, the following points can be concluded:

- The best results for angular interrogation mode (θ_{SPR}) were observed at d_{Ag} from 40 to 60 nm
- The SPR phenomenon was observed to be highly expressed in the visible range, commencing at 600 nm and improving further at 700 nm.
- The sensor's highest operating stability was found in the visible section of the spectrum at a wavelength of 600 nm. When used to detect changes in the RI of the aqueous medium with a change in RI of $\Delta n \geq 0.02$, the sensitivity ranged between $S = 134$ and 140. The length of the SPR dip (L_d) approached 0.9, and FWHM values ranged from 6.6° to 6.8^o at varying thicknesses of $d_{Ag} = 10 - 80$ nm.
- The suggested sensor may be employed as an effective biosensor in the visible spectrum areas (600 and 700 nm) with d_{Ag} of 40 to 60 nm.

Acknowledgments

The authors gratefully acknowledge the Department of Physics, College of Science, Mustaniriyah University, Baghdad, Iraq (www.uomustansiriyah.edu.iq), for their assistance with this study.

Nomenclatures

d_{Ag}	Silver film thickness, in nm
L_d	Surface plasmon resonance dip length, in nm
S	Sensitivity
Δn	The change in water refractive indices

Greek Symbols

λ_{SPR}	The propagation wavelength of the surface plasmon (nm)
θ_{SPR}	The surface plasmon resonance angle (degrees)

Abbreviations

FWHM	Full width at half maximum
SPR	Surface plasmon resonance
RI	Refractive index

References

[1] Ritchie, R.H., Phys. Rev., 106 (5) (1957) 874.

[2] Kittel, C., "Introduction to Solid State Physics", 8th Ed., (Wiley, Hoboken, NJ, 2005).

[3] Li, Y., "Plasmonic Optics: Theory and Applications", (SPIE Press, Bellingham, Washington, 2017).

[4] Zayats, A.V., Smolyaninov, I.I. and Maradudin, A.A., Phys. Rep., 408 (3-4) (2005) 131.

[5] Al-Qazwini, Y., Noor, A.S.M., Yadav, T. K., Yaacob, M.H., Harun, S.W. and Mahdi, M.A., Photonic Sensors, 4 (4) (2014) 289.

[6] Chen, S. and Lin, C., Optik 127 (2016) 7514.

[7] Lin, C. and Chen, S., J. Appl. Phys., 125 (11) 2019) 113101.

[8] Kadhum, F.J., Kafi, S.H., Saeed, A.A., Al-Zuky, A.A. and Al-Saleh, A.H., Sci. J. King Faisal Univ.: Basic Appl. Sci., 22 (2) (2021) 76.

[9] More, A.M., Kondawar, S.B. and Dongre, S.P., Jordan J. Phys., 15 (1) (2022) 1.

[10] Widayanti, Abraha, K. and Utomo, A.B.S, Biosensors, 8 (3) (2018) 75.

[11] Homola, J., Chem. Rev., 108 (2008) 462.

[12] Gupta, B.D. and Verma, R.K., J. Sens., 2009 (2009) 979761.

[13] Johnston, K.S., Karlsen, S.R., Jung, C.C. and Yee, S.S., Mater. Chem. Phys., 42 (1995).

[14] Kajenski, P.J., Opt. Eng., 36 (1997) 1537.

[15] Raether, H., "Surface Plasmons on Smooth and Rough Surfaces and on Gratings", (Springer, Berlin, 1988).

[16] Reitz, J.R., Milford, F.J. and Christy, R.W., "Foundations of Electromagnetic Theory", (Addison-Wesley, New York, 1993).

[17] Cardona, M., Am. J. Phys., 39 (1971) 1277.

[18] Rawwagah, F. Jordan J. Phys., 14 (2) (2021) 155.

[19] Yamamoto, M., Rev. Polarogr., 48 (3) (2002) 209.

[20] Špringer, T., Ermini, M.L., Špačková, B., Jabloňků, J. and Homola, J., Anal. Chem., 86 (20) (2014) 10350.

[21] Salamon, Z., Macleod, H.A. and Tollin, G., Biophys. J., 73 (1997) 2791.

[22] Homola, J., Sens. Actuators B, 41 (1997) 207.

[23] Deng, Y. and Liu, G., Procedia Eng., 7 (2010) 432.

[24] Seo, M., Lee, J. and Lee, M. Opt. Express 25(22) (2017) 26939.

[25] Rouf, H.K. and Haque, T., Prog. Electromagn. Res. M, 76 (2018) 31.